A low temperature ultrahigh vaccum scanning force microscope

Hans J. Hug, B. Stiefel, P. J. A. van Schendel, A. Moser, S. Martin, and H.-J. Güntherodt[a)]
Institute of Physics, University of Basel, Klingelbergstrasse 82, CH-4056 Basel, Switzerland

(Received 13 November 1998; accepted for publication 14 May 1999)

This article describes the design of a versatile ultrahigh vaccum (UHV) low temperature scanning force microscope system. The system allows scanning probe microscopy measurements at temperatures between 6 and 400 K and in magnetic fields up to 7 T. Cantilevers and samples can be prepared in UHV and transferred to the microscope. We describe some technical details of our system and present first measurements performed at different temperatures and in various scanning force microscopy operation modes. We demonstrate distortion free and calibrated images at temperatures ranging from 8 to 300 K, atomic resolution on NaCl at 7.6 K and various magnetic force microscopy images of vortices in high transition temperature superconductors. It is demonstrated that our instrumentation reaches the thermodynamically determined sensitivity limit. Using standard cantilevers force gradients in the 10^{-6}N/m range, corresponding forces of about 10^{-15}N can be measured. © *1999 American Institute of Physics.* [S0034-6748(99)00909-0]

I. INTRODUCTION

Despite many successful low temperature scanning tunneling microscopy experiments[1] the number of results obtained by low temperature scanning force microscopy is still small.[2] Furthermore, no commercial manufacturer has presented a low temperature scanning force microscope (LTSFM) so far,[3] although several low temperature scanning tunneling microscope (LTSTM) systems are available.[4–7] An important reason is that an SFM requires a sensor to measure the deflection of the cantilever. This sensor has to operate at low temperatures and the relative position of the cantilever and the deflection sensor has to be adjustable or remain within the operation range of the deflection sensor at all temperatures. The large temperature difference (up to 300 K) upon cooling may cause lateral drifts larger than the dimensions of the cantilever and a vertical motion of the cantilever up to several tens of microns. We have found that the vertical motion of the cantilever is mainly due to a bending caused by the difference in expansion coefficients of the cantilever material and the coating needed to perform a specific experiment.[8] This problem can be solved by an appropriate coating of the cantilever or by choosing a deflection sensor which is either adjustable or not disturbed by large vertical position offsets of the cantilever. In literature we find a large variety of sensors which have been used in LTSFM instrumentation. Below we give a brief historical overview on LTSFM instrumentation, describing designs using tunneling,[9,10] fiber-optic interferometry,[11–16] piezoresistive cantilevers,[17] and laser beam deflection.[18]

The first successfully working LTSFM built by Gießibl *et al.*[9] was equipped with a tunneling tip as deflection sensor. However, besides some work on single crystalline potassium bromide[19] no further results obtained with this instrument have been published. The alignment problem of the deflection sensor with respect to the cantilever is most severe when this method is used. The position of the tunneling tip has to be maintained within fractions of an Angstrom during operation and the tunneling tip has to be approached within the working range of the piezo which controls the tunneling tip-to-cantilever distance. Furthermore, the tunneling junction might suffer from contamination and the microscopic structure of the cantilever backside might severely influence the image process.[20] Another instrument using tunneling to measure the cantilever deflection has been described by Volodin and Marchevsky.[10] Again, besides very preliminary magnetic force microscopy data on $Bi_2Sr_2CaCu_2O_{8+x}$ (BSCCO) no further results have been obtained. Note that despite these severe problems, the tunneling sensor might become important for ultralow temperature instruments, since it dissipates very little energy (see Ref. 15).

After the invention of the fiber optic interferometer as deflection sensor[21,22] many groups have implemented this type of deflection sensor in their instrumentation.[11–16] The adjustment of the cantilever to the fiber end is less critical than in the case of a tunneling sensor. Furthermore, only a single fiber has to be introduced into the cryostat. All optical and electronic components associated with the fiber optic interferometer are located outside the cryogenic environment of the microscope. A first implementation of such a sensor in a LTSFM is described in Ref. 11. Albrecht *et al.* have successfully imaged the topography of a single crystalline $Bi_2Sr_2CaCu_2O_{8+x}$ sample and bits written on a magneto-optic recording medium at room temperature and at 5 K. Further several attempts were made to image vortices on both $NbSe_2$ and $Bi_2Sr_2CaCu_2O_{8+x}$, but no unambiguous images of vortices were obtained.[23] We have used a similar fiber optic interferometer[24] as a deflection sensor for our first low temperature scanning force microscopy instrumentation.[12] We have then measured the levitation force[25] on $YBa_2Cu_3O_{7-x}$ (YBCO) single crystals cooled with and without an applied external field[26] and imaged

a)Electronic mail: hug1@ubaclu.unibas.ch

single vortices using a low temperature magnetic force microscope (LTMFM) for the first time.[27] Furthermore, we have used the magnetic stray field of the tip to nucleate vortex bundles.[28,29]

Moloni *et al.*[13] have also built a LTSFM with a fiber optic interferometer as deflection sensor. Their instrument is coupled via N_2 exchange gas to a liquid nitrogen (LN_2) cryostat and was used to study the domain structure in single crystal magnetite. Then Euler *et al.*[14] have presented an interferometer based variable temperature scanning force microscope which is cooled by a He gas flow or by direct immersion into LHe. The system was used to image the topography of a magneto-optical disk at room temperature, 77 (using LN_2) and 4.2 K (using LHe). Intermediate temperatures are reached only by making use of the slow warm up after having removed the coolant. Furthermore, the topography of a YBCO thin film sample was imaged at 7.8 K but no MFM images on this or any other samples have been presented. Allers *et al.*[16] have presented the first fiber optic based LTSFM working in ultrahigh vacuum (UHV), with a lowest reachable temperature of 9 K. However this temperature is not measured at the location of the sample but at the bottom of the instrument facing the cold bottom of the cryostat insert. The system features a cryostat with a LHe container of almost 100l and allows an operation time without refill of three days. The cool-down from room temperature to 10 K takes a total of 20 h. The cryostat does not contain a magnet system and allows variable temperature operation only during the warm-up process. With this instrument the imaging of atomic periodicity on highly oriented pyrolytic graphite (HOPG) was demonstrated in contact mode at 77, 40, and 10 K. Further room temperature measurements in a dynamic noncontact operation mode have been presented revealing atomic resolution on a single crystal of InAs. Pelekhov *et al.*[15] have presented the first fiber optic LTSFM working inside the mixing chamber of a dilution cryostat achieving a minimum temperature of 30 mK and a magnetic field up to 9 T. Their LTSFM also contains an *xy* motor for macroscopic positioning of the cantilever with respect to the sample. However, the extreme condition of immersing the cantilever in the normal/superfluid helium mixture limits the measurement modes to the contact modes and leads to a high noise level. In spite of these restrictions, measurements revealing atomic steps on HOPG at 4.2 K and an image of a mesoscopic Au ring of 1 μm diameter at 30 mK and in a field of 9 T have been presented.

An alternative approach for the measurement of the cantilever deflection is to use piezoresistive cantilevers. At a first glance such a sensor seems to be ideal, since it converts an LTSTM to an LTSFM simply by replacing the tunneling tip by the piezoresistive cantilever avoiding potential alignment problems of cantilever and deflection sensor. However, the disadvantages of this approach are a limited range of cantilever force constants and resonance frequencies and potential technical difficulties if UHV preparation of the cantilevers is intended. Furthermore, the energy dissipated in the cantilever is considerable.[30,31] Despite these difficulties Yuan *et al.* have presented an LTSFM using such a sensor.[17] They have used their instrument to study high temperature superconductors (HTSC)[32] and colossal magneto resistive materials.[33] However, the results on HTSC remain rather ambiguous.[34] Convincing results using an LTSFM with piezoresistive detection have been presented recently by Volodin *et al.* in Ref. 35. In their work they have used higher-flexural modes to enhance the sensitivity of their instrument[31] to image vortices in $NbSe_2$ single crystals.

Finally, also laser beam deflection, which is the most popular deflection sensor for room temperature SFM, has been used for LTSFM instrumentation by Prater *et al.*[36] and Dai *et al.*[18] Although this method is commonly used for instruments working under ambient and UHV conditions, the cooling of a beam deflection type SFM remains a challenge. One of the remaining problems is the alignment of the beam deflection system to the cantilever during and after the cool-down process. This alignment has to be done fully remote controlled and without optical access to the microscope. Furthermore, the photoelectronics and preamplifier are located in UHV and at low temperatures. To overcome the above difficulties both instruments[36,18] use a cold-finger to cool the sample, whereas the rest of the instrument remains uncooled. The disadvantages are an inhomogeneous temperature distribution within the microscope, only moderately low temperatures (140 K in Prater's and 100 K in Dai's instrument), and possibly a contamination of the sample.

The large variety of possible designs of LTSFM instruments makes it rather difficult to compare the performance of different instruments. We strongly suggest that besides atomic resolution, the minimal z derivative of the force[37] is measured. Obviously, this quantity should not depend on a specific LTSFM design or on the vacuum enviroment used but is given solely by the measurement temperature, the bandwidth and the properties of the cantilever (force constant c_L, quality factor Q, resonance frequency f_0) which is used. Note that, this for many of the above designs has either not been done or the thermodynamical limit was missed by orders of magnitude.

II. SYSTEM DESIGN

The LTSFM system presented here, allows force and/or tunneling measurements in ultraghigh vacuum (UHV) at temperatures between 6 and 400 K and in magnetic fields up to 7 T. Cantilevers and samples can be prepared in UHV and transferred to the microscope. We have met these, often contrary requirements with a completely new SFM design. The microscope is described in the following subsection. The UHV system is described in Sec. II B whereas the details of the cryostat are discussed in Sec. II C.

A. Microscope

Our new LTSFM is designed to allow multimode SFM operation in UHV, at low temperatures and in high magnetic fields using fiber-optic interferometry as sensor for the cantilever deflection. The main design criteria were a small size, a high modularity and geometrical symmetry, and the sole use of nonferromagnetic materials (even the electrodes of the piezos are made out of Cu instead of the more usual Ni).[38] The size restrictions arise from the 50 mm inside diameter of

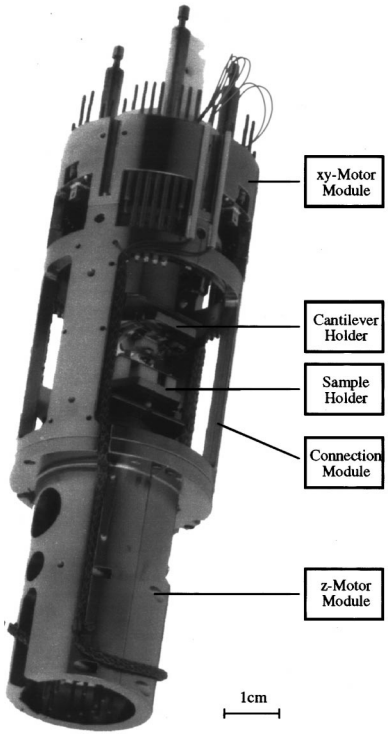

FIG. 1. Low temperature SFM/STM compatible with UHV and high magnetic fields.

the variable temperature insert (VTI, see Sec. II C) which is fitted into the superconducting solenoid (ID: 77 mm). The combination of these severe restrictions in size with full UHV functionality (i.e., *in situ* cantilever/sample exchange) and *xy* positioning[39] is a major design challenge. Our solution to this challenge is a modular force microscope with only 40.4 mm outside diameter and 157.5 mm length (Fig. 1).

The small size, the symmetrical geometry and the thermal compensation of some critical parts lead to a high mechanical stability and a reduced relative thermal drift of the cantilever-to-fiber position and the cantilever-to-sample position. The modularity (see Fig. 2) allows easy maintenance and possible later adoptions to meet new experimental needs. Therefore, many modules and components of the design have been used directly or only with minor modifications in

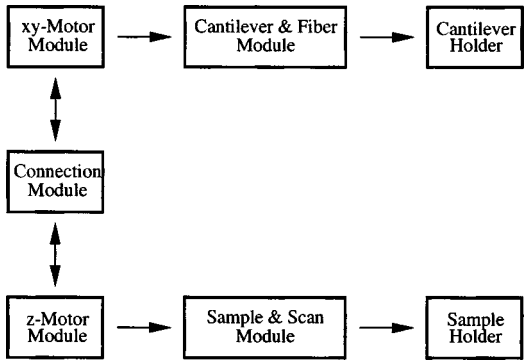

FIG. 2. Schematic view of the microscopes modularity. Note that each module is a functional entity, which can be easily exchanged as a whole when broken or can be replaced by a different module giving another functionality.

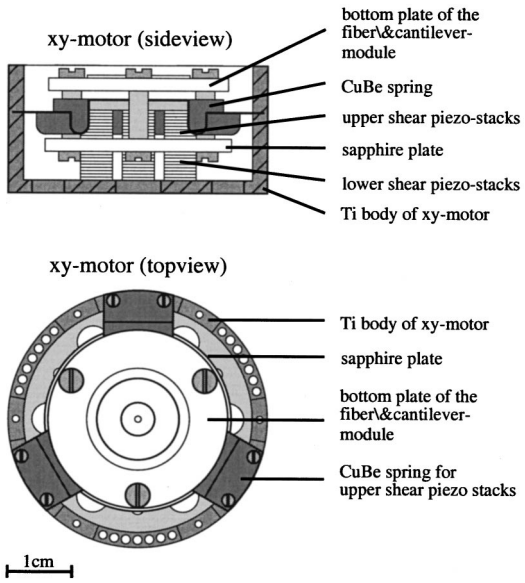

FIG. 3. Principle of the *xy* motor.

many other instruments.[40–44] The titanium body of our instrument consists of an *xy motor module* attached to one end of a *connection module* and a *z motor module* mounted to the other end.

1. Connection module

The connection module mechanically and electrically interconnects the *xy* motor module with the *z* motor module. Large windows in the connection module allow the exchange of the sample/cantilever by a mechanical hand[45] when the microscope is moved to the manipulation position inside the SFM chamber (see Sec. II B 2). Furthermore, these windows offer a view of the cantilever and sample from the $\pm X$ and $\pm Y$ directions.[46] The tip of the cantilever can be seen from two orthogonal directions with a lateral/vertical viewing angle of 90°/78° in $\pm Y$ directions (view along the axis of the cantilever from its tip to the mounting chip) and with 29°/78° in $\pm X$ directions. However, the viewports of the SFM chamber reduce the total viewing angle from the outside of the chamber to 72°/72° in $+Y$ direction and 29°/30° in $+X$ direction. This allows to use the piezo motors of the SFM to approach the tip to a specific sample location under the optical control of a binocular microscope with a high magnification and a stereoscopic view.

2. xy motor module

The *xy* motor basically consists of a sapphire plate which is clamped between two groups of three shear piezo stacks (Fig. 3). Each stack consists of eight shear piezo plates to move into the *x* and *y* direction and to compensate for the sensitivity loss of the piezo plates at low temperatures. The *xy* motor can be operated either in the inertia mode with all the piezo stacks moving simultaneously or in the friction mode with the piezo stacks moving one after the other. The motor generates a considerable force of typically 5 N. The range of motion is geometrically limited to a circle with a

diameter of 7 mm. This is the maximum range achievable for the outside diameter of 40.4 mm, a wall thickness of 2.4 mm,[47] 5 mm sized shear-piezoplates, and the fiber running through the center of the motor. The minimum step size is around 20 nm (see Sec. III A). The maximum speed depends on the output voltage and step repetition frequency of the driver electronics. We typically reach 230 μm/s using the Omicron driving electronics[48] at room temperature. The *xy* motor module includes the *fiber&cantilever module* which is mounted on the top of the sapphire plate. The fiber&cantilever module consists of a fiber piezo to adjust the fiber-to-cantilever distance and a *cantilever holder support*.

This support is a precise kinematic mount into which a cantilever fixed to a *cantilever holder* is introduced. The position of the cantilever on this holder and thus, the cantilever-to-fiber position is adjusted *ex situ* by means of a dummy stage. The dummy stage precisely reproduces the relative distances between the fiber end and the support positions of the kinematic mount. After this adjustment the cantilever holder is introduced into the UHV system and transported to the SFM. Due to the thermally well compensated construction of the cantilever holder and the cantilever-holder support no further coarse adjustment is needed in the SFM. Fine adjustments can be made by means of the fiber piezo. The cantilever holder also contains a small piezo plate located just below the cantilever. This piezo plate is used to drive the cantilever oscillation in the dynamic operation modes.

Furthermore, we have a total of four electrical connections to the cantilever holder. They are used for applying a voltage to the cantilever, to drive the cantilever-oscillation piezo and for other purposes. In addition, the fiber end can be set to an arbitrary potential. The inhomogeneous field between the gold cladding of the fiber and the cantilever then changes the force constant of the cantilever. This allows force constant controlled operation modes as proposed by Jarvis *et al.* in Ref. 49. In contrast to our method which relies on electrostatic forces, Jarvis *et al.* have used a magnetic field gradient interacting with a magnetic particle mounted onto the cantilever.

3. z-motor module

The *z*-motor module consists of a hexagonal sapphire prism with a large central bore (Fig. 4). The prism is clamped between two groups of three shear piezo stacks, each consisting of four shear-piezo plates. The motor generates a considerable force around 5 N which is by far large enough to move the prism, the scan piezo and the sample against gravitation. The scan piezo is mounted into the inside of the hexagonal sapphire prism. This reduces the total length of the instrument. The length of the *z*-motor module which includes the *z* motor and the 38.1-mm-long scan piezo is only 69 mm. A *sample-holder support* is mounted on the top of the scan piezo. A *sample holder* can be inserted into the sample-holder support. The sample holder and the sample-holder support are constructed similar to the cantilever holder and cantilever-holder support. Thus, the sample holder can be mounted with the same precision as the cantilever holder. This allows to refind a specific sample area after having removed and reinserted the sample holder (see Fig. 11), i.e., after a next step of sample preparation. The sample-holder support also contains a resistive heater and a temperature sensor (see Sec. II C 3).

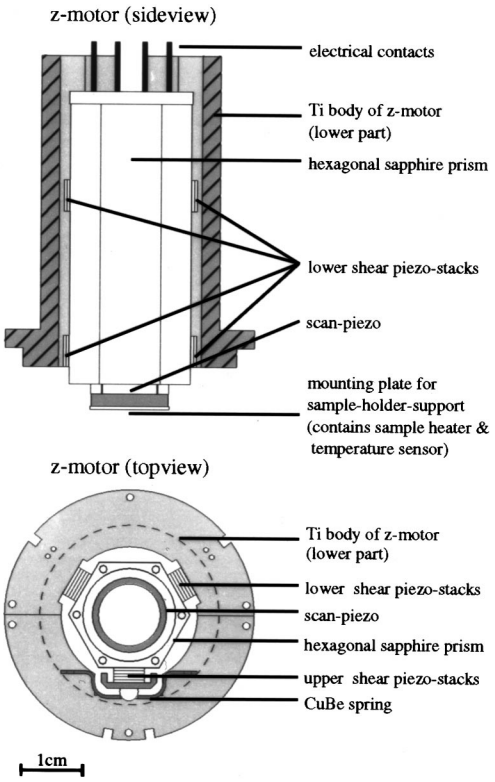

FIG. 4. Principle of the *z* motor.

4. Sample holders

As described above, a sample holder can be inserted into the sample-holder support (Fig. 5). There are four electrical contacts to the sample holder (only two of them are shown in the drawing). We have presently built three different types of sample holders making different use of these electrical contacts.

a. Regular sample holder. The sample is glued on a ceramic plate with four electrical contact pads. These can be used to bond wires to the sample, e.g., for resistive four-contact measurements. The ceramic plate is then screwed to the sample holder connecting the contact pads of the plate with the electrical contacts of the holder.

b. Cantilever-type sample holder. As mentioned in Sec. II A 3 the construction of the kinematic mount of the sample-holder support and the cantilever-holder support is equal. Thus, a small magnetic sample mounted on a cantilever can be inserted in both positions into the sample-holder support or the cantilever-holder support. In the first case, which is the normal force microscopy measurement configuration, the sample is scanned by the tip of a second cantilever inserted into the cantilever-holder support. In the second case the sample which is mounted onto a cantilever is inserted into the cantilever–holder support position. Then, the magnet system of the cryostat is used to generate a homogeneous

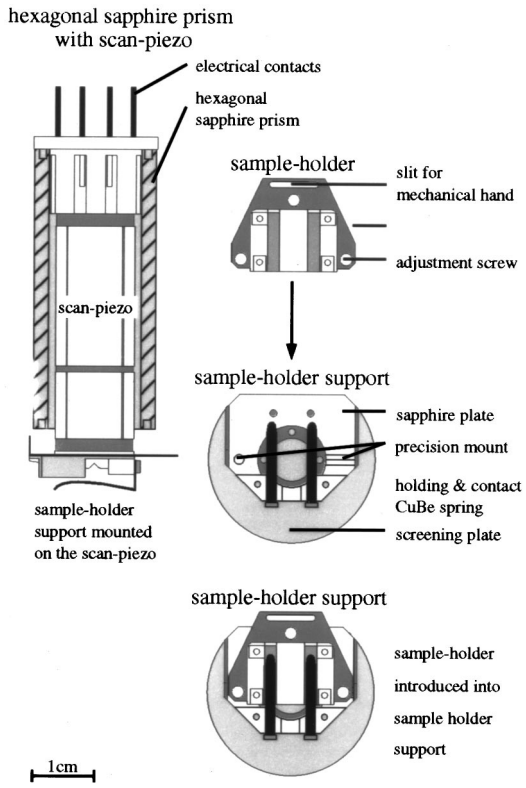

FIG. 5. Principle of the sample-holder system.

magnetic field to define the magnetic state of the sample and a gradient field is used to generate a force acting on the magnetized sample. The bending of the cantilever then is a measure for the magnetization of the sample (see Sec. II C 4). Without the magnetic field gradient, the magnetostriction of a thin magnetic film deposited onto the cantilever could be measured. Similarly, the latent heat of phase transitions of the sample could be used to give rise to a bending of a thermally sensitive cantilever.[50–52]

c. Heatable sample holders. Standard UHV-sample preparation includes sample heating. For this purpose we have constructed two types of heatable sample holders. One type heats the sample by passing a current directly through the sample. The second type passes a current through a resistive meander pattern molybdenum resistor sandwiched between two thin aluminum-oxide plates onto which the sample is mounted. In both cases the two other electrical contacts are used for a thermocouple to measure the sample temperature.

B. UHV system

The UHV system consists of two main groups of UHV chambers. One for sample/cantilever preparation and standard surface science analysis and one for the microscope handling and sample/cantilever exchange. A schematic sideview of the whole UHV system is shown in Fig. 6.

1. Preparation and analysis chamber system

The system consists of a fast entry air lock (FEAL), a *preparation chamber* and an *analysis chamber*.

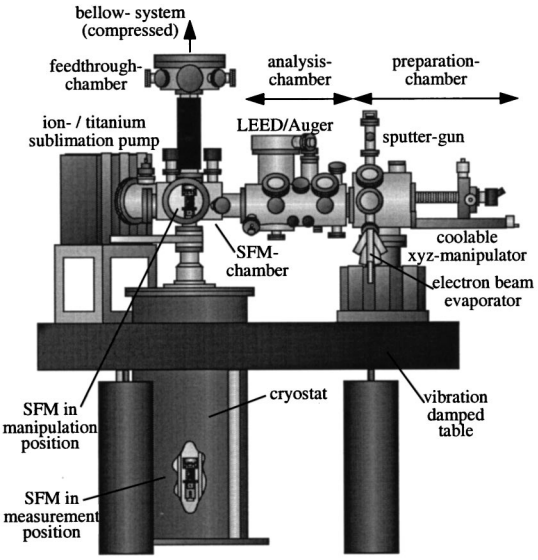

FIG. 6. Sideview of the UHV system.

A sample/cantilever mounted on a specific holder (see Sec. II A 4) is introduced into the UHV chamber system through the FEAL.

For standard UHV cleaning and preparation the sample/cantilever holder is inserted into the sample/cantilever-holder support of a *preparation head*. The support is equivalent to the one of the microscopes. Thus it precisely defines the position of the sample/cantilever holder and supports four electrical contacts to the sample/cantilever holder. These contacts can be used to heat the sample and measure its temperature when a heatable sample holder (see Sec. II A 4) is used. The preparation head has two further holder supports allowing the insertion of shutter holders. The construction of these supports is similar to the one of the sample/cantilever-holder support of the microscope. Again it precisely defines the positions of shutter holders relative to the sample/cantilever holder. Therefore it is possible to mask well defined areas of the sample/cantilever from preparation. Note that the shutter holders can be introduced in or transported through the UHV system similarly to the sample/cantilever holders. The relative positioning of the shutter with respect to the sample/cantilever is performed *ex situ* by means of a dummy stage.

The preparation head itself is mounted to the coolable linear/rotary manipulator[53] of the preparation chamber. This manipulator then transports the preparation head to the preparation position. In this position the preparation head can be rotated such that the sample/cantilever faces a sputter gun,[54] a triple electron beam evaporator[55] or future preparation devices, e.g., a sample cleaver.

After the cleaning/preparation procedure the sample is transferred from the linear/rotary manipulator to the linear transport system of the analysis chamber. The sample/cantilever holder can then be moved to the low-energy electron diffraction (LEED)/Auger system, to sample/cantilever-holder storage places or directly into the microscope-handling chamber system.

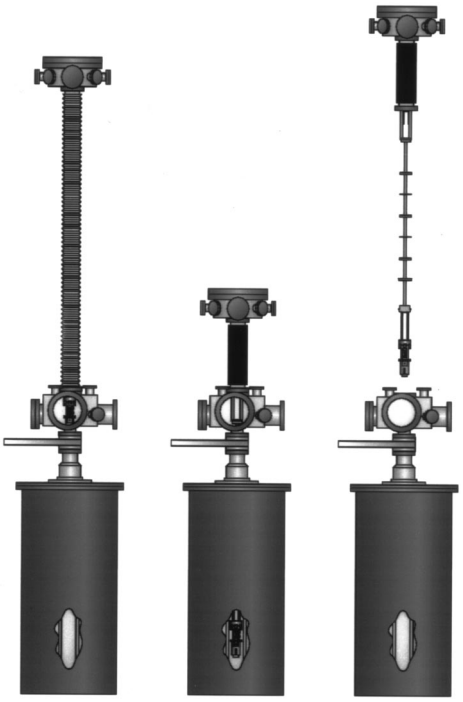

FIG. 7. Working positions of the SFM. Left: Manipulation position for cantilever and/or sample exchange (flexible bellow fully elongated). Middle: Cooling and measurement position (flexible bellow fully compressed). Right: Service position that gives free access to the SFM and the cryostat insert (flexible bellow fully compressed but detached from SFM chamber).

2. Microscope-handling chamber system

The purpose of this chamber system is the sample/cantilever exchange between the microscope and the transport system of the analysis chamber and the vertical transportation of the microscope between its different operation positions (see below).

The microscope-handling chamber system consists of the *SFM chamber*, the UHV tube of the cryostat (see Sec. II C 2) and the *feedthrough chamber*, which is connected to the SFM chamber by flexible bellows and a sophisticated vertical translator.

The SFM is spring suspended to the bottom of a cryostat insert whereas the cryostat insert itself is attached to the feedthrough chamber. All electrical connections to the microscope and the optical fiber are guided along the insert from the feedthrough chamber to the SFM.[56]

The vertical translator moves the feedthrough chamber, the cryostat insert, and the SFM between three working positions (Fig. 7):

(1) Manipulation position: In this position the SFM is located in the center of the SFM chamber and fixed by two rotatable clamps to allow a sample or cantilever exchange.[57] The sample/cantilever holder is then transferred to the SFM by a mechanical hand.[45] The mechanical hand can be rotated such that the cantilever and sample supports of the microscope can be reached without further vertical adjustments. In the manipulation position two windows allow the observation of the cantilever/sample from two orthogonal directions with very high vertical and horizontal viewing angles (see Sec. II A 1). Thus the manipulation position is for an optically controlled positioning and approach of the cantilever to the sample.
(2) Cooling position: After the insertion of the sample/cantilever into the SFM, it can be lowered to the cooling position (see Sec. II C 2). At the bottom position the conical end of the cryostat insert locks into its counter part. Thus the weight of the feedthrough chamber, the cryostat insert, and the air pressure generate a force of about 1000 N, which presses the conical end of the insert into its counterpart. This large force is necessary to achieve a good thermal contact without using exchange gas.[58,59]
(3) Service position: In this position the SFM hangs, freely accessible, above the SFM chamber. To reach this state the bellow is first compressed, fixed with steel cables and dismounted at the SFM chamber. Then the vertical translator is moved beyond the manipulation position to lift the SFM above the top flange of the SFM chamber.

3. Pumping system

During the SFM measurement process no mechanical pumps are running to avoid vibrations. In this case the vacuum is achieved by two ion pumps with a pumping speed of 200l/s each. These ion pumps contain a titanium evaporator and coolable getter shields which increase the pumping speed to 1000l/s.

During sample preparation, especially during sputtering (with relatively high Ar background pressure) the preparation chamber is pumped by an additional turbo pump. We use a wide range turbo molecular pump with a high compression ratio even for light noble gases. Furthermore, we have installed another wide range turbo molecular pump which is attached to a manifold ending in several full metal valves. They lead to the following chambers:

(1) SFM chamber. The chamber can be prepumped by the turbo through a flexible bellows connector.
(2) Analysis chamber. The manifold is attached to a CF63 full metal valve which is mounted to the analysis chamber. The turbo is used for prepumping or when the analysis chamber is contaminated with argon from sputtering.
(3) FEAL. The fast entry air lock is pumped through a flexible hose.
(4) Sputter gun and argon gas line. The sputter gun can be pumped differentially for a better beam quality.
(5) Outer vacuum chamber (OVC) of the cryostat.[60] A flexible hose leads to a KF[61] valve battery to set the He-gas pressure inside the OVC. The prepumping is done by a membrane pump which gives a carbo-hydrogen free vacuum that avoids a contamination of the cooled cryostat volumes.

C. Cryostat

The cryostat was custom designed by Oxford Instruments.[62,63] It is a superinsulated bath cryostat with a UHV compatible, variable temperature insert (VTI), and a superconducting magnet system.

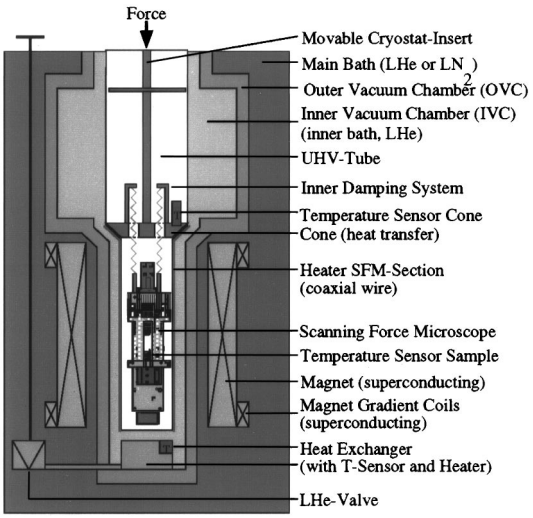

FIG. 8. Schematic view of the cryostat. The UHV tube (white) contains the microscope that is spring suspended from the cryostat insert. The cryostat insert is shown in the cooling position. The OFHC copper cone is pressed into its cooled counterpart providing a good thermal contact. The UHV tube is surrounded by the inner vacuum chamber (IVC) and the outer vacuum chamber (OVC) which allow to define the thermal connection between the cryogenic liquid in the main bath and the wall of the UHV tube. For this purpose IVC and/or OVC can be either evacuated or filled with exchange gas or LHe (IVC only). Furthermore, the LHe needle valve and the heat exchanger are shown. Finally the superconducting part of the magnet system is shown (high-field and gradient-field coils).

1. Mechanical construction

Particular care was taken to reduce the generation of mechanical noise. The superinsulated cryostat does not require LN_2 for thermal shielding and the low heat loss construction minimizes the LHe consumption and thus the bubbling noise.

Furthermore, the high mechanical stiffness of the VTI does not amplify mechanic and acoustic vibrations. The thin walled VTI containing the SFM is located in the center of a triangle formed by three other tubes. These are used to support the liquid He (LHe) level sensor, the power lines to the superconducting solenoid and, the electrical connections to the gradient and normal conducting coils (see Sec. II C 4). The mechanical stability is increased by interconnecting these tubes with rigid baffles used for radiation screening of the main coolant bath.

Usually, the superconducting magnet system is mounted at the bottom of the VTI. In our construction the magnet system is attached to the bottom of the cryostat. This reduces the mass at the end of the VTI and thus increases its resonance frequency.

2. Cryogenic construction

The variable temperature insert (VTI) of the bath cryostat consists of three concentrical tubes, various heaters and temperature sensors, a needle valve and the movable cryostat insert (Fig. 8).

The moveable cryostat insert consists of a central stainless steel tube supporting baffles and thermal grounding points for the wires at four different height levels. The bottom of the cryostat insert ends in a truncated cone made out of OFHC[64] copper. The SFM is spring suspended from this cone. An eddy current damping system is installed above the cone, outside the area of strong magnetic field. The thermal connection of the SFM to the cone is achieved by copper braids. The cone contains a RhFe temperature sensor and serves as a temperature reference point of the SFM. A second truncated cone of slightly larger diameter is located about 15 cm above the first one. The vertical distance between the cones can be changed by pressing the upper cone upwards against a stiff spring.

The cryostat insert is moved by the vertical translator to lift the SFM between the manipulation position inside the SFM chamber and the cooling position (see Sec. II B 2). In this position the cryostat insert is fully inserted into the innermost (*UHV tube*) of the three concentrical tubes of the VTI (see Fig. 8).

The UHV tube is attached to the SFM chamber via a gate valve. The two further tubes surrounding the UHV tube form two volumes, the *inner vacuum chamber* (IVC) and the *outer vacuum chamber* (OVC) which separate the UHV tube from the cryogenic liquid in the main bath. Both volumes, the IVC and OVC can be pumped or filled with exchange gas. Furthermore, the IVC can be filled with gas or liquid from the main bath via a *needle valve* and a *heat exchanger* controlling the temperature of the flowing medium. To improve the temperature control of the UHV tube it is surrounded by two coaxial heating wires. One of them, *the bake-out heater*, winds around the whole length of the UHV tube and is used to bake it. The other one, *the cone heater*, is located only at the bottom part of the UHV tube to precisely control the temperature of the SFM. The two volumes (IVC and OVC), the different heaters, and the needle valve allow various cryogenic operation modes (see Sec. II C 3).

The top end of the UHV tube is formed by a conflat flange with an inside diameter of 70 mm. The inside diameter of the UHV tube is then reduced twice to the final 50 mm towards the bottom end. The two diameter reduction pieces are made out of OFHC copper and serve as contact counter-parts for the two OFHC copper cones of the cryostat insert which can be moved by the vertical translator. The 50 mm diameter section of the UHV tube (*SFM section*) contains the microscope if the vertical translator is moved to the cooling position. To increase the temperature uniformity of the SFM section, copper strips are soldered to its outside.[65]

If the insert is lowered into the UHV tube of the cryostat the upper cone locks into its counter-part inside the tube. This cone takes most of the heat load coming from the wires and the insert itself. When the insert is lowered a few millimeters more, the bottom cone also locks into its counter-part. This cone makes the thermal connection of the SFM inside the UHV tube and the cooled part of the cryostat outside the UHV tube.

3. Cryogenic operation

Once the SFM is cooled, the temperature of the sample can be controlled by a heater and a temperature sensor located inside the microscope, just below the sample. This heater allows rapid changes of the sample temperature, e.g., to drive the sample through phase transitions. However, this

sample heater is not generally used for variable temperature measurements because it generates an inhomogeneous temperature distribution inside the SFM. Instead we use the variable temperature capabilities of our cryostat to define the temperature of the whole SFM section of the UHV tube. If the SFM is located in the cooling position, the cones of the cryostat insert provide a good thermal connection between the SFM, inside the UHV, and the outside of the SFM section of the UHV tube. Thus the microscope is in a homogeneous temperature environment. In the following we describe the details of the different cryogenic operation modes:

(1) Bake-out process of the cryostat: Usually UHV systems require a baking of the chambers to achieve a pressure below 10^{-10} mBar. In our case, a part of the UHV system, namely the UHV tube, is inside the cryostat. As described above, it is surrounded by a coaxial bake-out wire. During the bake-out process the heat conductivity to the main bath is minimized by pumping the IVC and OVC to a vacuum below 10^{-6} mBar. Additionally LN_2 is filled into the main bath of the cryostat to prevent the damage to the magnet system. Furthermore, the bake-out heater is useful, if a rapid heating up of the whole SFM section to room temperature is required.

(2) Exchange gas mode: In this mode, exchange gas in the IVC and OVC is used to adjust the heat conductivity between the SFM section of the UHV tube and the cooling liquid of the main bath. The exchange gas pressure defines the cooling speed and the base temperature of the SFM. Higher temperatures are achieved by using the cone heater. Note that the heater is outside the UHV, whereas the temperature sensor is fixed at the cone of the cryostat insert, located inside the UHV. The exchange gas mode has proven useful only if LN_2 is used as a coolant. In this case we reach a minimum base temperature of the sample inside the microscope of 78.6 K[66] using an exchange gas pressure around 300 mBar in IVC and OVC. An even lower temperature can be reached by pumping the LN_2 in the main bath solid.

(3) Gas flow mode: LHe[67] is taken from the main bath, guided through the needle valve to the heat exchanger inside the IVC. The OVC is evacuated to insulate the IVC from the main bath. In this mode the base temperature of the SFM is adjusted by controlling the pressure and the temperature of the flowing gas. The first is set by the position of the needle valve and the external pumping speed. The second is defined by the temperature of the heat exchanger. Again, temperatures above the base temperature are achieved by the cone heater. This operation mode requires two temperature controllers, one defining the temperature of the He gas and the other one defining the temperature of the SFM environment. In this mode we reach a minimum base temperature of the sample located in the SFM of 7.0 K using a He-gas pressure of 12 mBar with a temperature of 1.5 K of the heat exchanger.[68]

(4) Single shot mode: In this mode the IVC is filled with LHe by pressurizing the main bath and opening the needle valve. Note that the IVC widens to form a volume of about 1.5l. Again the OVC is evacuated to insulate the inner bath from the main bath. After closing the needle valve, temperatures below 7.0 K are reached by pumping on the inner bath only. This mode consumes a relatively large amount of LHe.

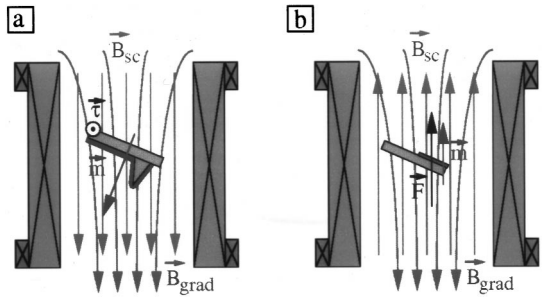

FIG. 9. (a) Shows that a torque, $\boldsymbol{\tau}$ (pointing out of the paper plane), acts on the cantilever even in a homogeneous magnetic field, $\mathbf{B}_{SC}$, if the cantilever magnetization, $\mathbf{m}$, is not fully aligned with the field. The gradient field, $\mathbf{B}_{grad}$, can be used to compensate $\boldsymbol{\tau}$. (b) A magnetic sample (red) is mounted on a kind of cantilever. The homogeneous field, $\mathbf{B}_{SC}$, defines the sample magnetization, $\mathbf{m}(\mathbf{B}_{SC})$, whereas the gradient field, $\mathbf{B}_{grad}$, generates a measurable force, $\mathbf{F}(\mathbf{m},\mathbf{B}_{grad})$, to determine the sample magnetization.

4. Magnet system

The magnet system used in our instrumentation consists of

(1) a superconducting solenoid for fields up to 7 T along the vertical direction (z axis) with a homogeneity of $1{:}10^5$ within 1 cm^3,
(2) a gradient coil to achieve a magnetic field gradient of 0.12 T/m (at 20 A driving current) along the z direction,
(3) a conventional solenoid producing a field of up to 28 mT (at 2 A driving current) along the z direction.

The superconducting solenoid and the gradient coils are designed to be used with LHe as a coolant only. In contrast, the normal conducting solenoid is used for producing small fields for measurements with LN_2 as a coolant or for fast field variations. Further, magnetic cantilevers deflect even in a homogeneous field, when the magnetization axis does not coincide with the axis of the applied field. In such a case the torque acting on the cantilever is

$$\boldsymbol{\tau} = \mathbf{m} \times \mathbf{B}_{SC}, \tag{1}$$

where $\mathbf{m}$ is the magnetic moment of the cantilever and $\mathbf{B}_{SC}$ is the field of the superconducting solenoid [see Fig. 9(a)]. This torque may lead to a large motion or even a destruction of the cantilever. Even an only 10-nm-thick and 40 μm by 40 μm large layer of iron on the flat area at the tip end of the cantilever generates a torque corresponding to force of some hundreds of nanonewtons acting at the end of the cantilever [Fig. 9(a)]. We plan to use the gradient field to compensate for the torque induced motion of the cantilever.

Furthermore, the gradient field can be used to measure the magnetization of the ferromagnetic layer on the cantilever or of a sample mounted on a kind of a cantilever [Fig. 9(b)]. The high sensitivity of the force measurement gives an excellent resolution of the magnetic moment.

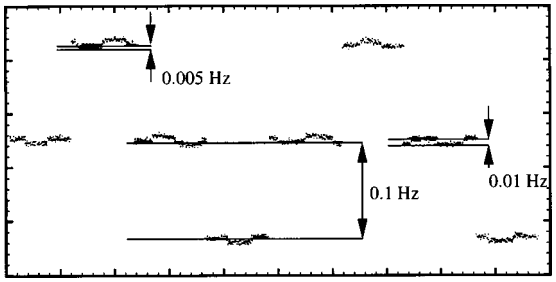

FIG. 10. The output signal of the analog FM detection system is shown for an input signal of 500 kHz varying with steps of 0.1 and 0.01 Hz, respectively.

$$\mathbf{F}=\mathbf{m}(\mathbf{B}_{SC})\cdot\frac{\partial B_{SC,z}}{\partial z}. \tag{2}$$

With a minimal measurable force of 10^{-12} N a field gradient of 0.12 T/m we reach a magnetic moment sensitivity of $8.3\times10^{-12}\,\mathrm{Am}^2$. This sensitivity is about three orders of magnitude better than the one of a vibrating sample magnetometer, but about two orders of magnitude worse than the one of a superconducting quantum interference device (SQUID) magnetometer.[69] However, the sensitivity of such a cantilever-type magnetometer could easily be improved by using the dynamic measurement modes or by implementing a different magnet system with stronger gradient coils. Indeed cantilever type magnetometers are now commercially available.[70]

III. MEASUREMENTS

As described in the previous sections on the SFM instrumentation, our new SFM is well suited to perform measurements in the various static (dc) and dynamic (ac) modes of measurement.

In the dc modes the static deflection of the cantilever is detected (We have given a comprehensive description in Refs. 71,72). The feedback system then is either switched to the z direction of the scan piezo (constant-force mode) or to the fiber piezo (variable deflection mode). The first requires a tip-sample interaction with a derivative which does not change its sign during the scanning process.[73] The second does not require any special type of interaction between the tip and the sample because the feedback controls the fiber-to-cantilever distance directly. Thus the variable deflection mode is well suited to measure force versus distance curves or images where the interaction force gradient changes its sign within the image.

In the ac modes the cantilever is oscillated by a small piezo plate located inside the cantilever holder about 2 mm below the cantilever. Either a lock-in amplifier or an analogue (similar to Ref. 37) or digital[74] FM detector is used to detect amplitude or phase of the forced cantilever oscillation. The analogue FM detector is able to measure frequency shifts as small as 0.005 Hz (see Fig. 10).

A. Test of sample exchange and *xy* motor

The described test of the reproducibility of the sample and cantilever exchange was performed under ambient conditions. However, we have later found that UHV operation makes no difference in any of the experiments described below. We have imaged a compact disk sample using the variable deflection mode with the tip in contact with the sample [Fig. 11(a)]. Afterwards the sample was retracted about 1 cm, removed from the SFM, reinserted into the SFM and reapproached to the tip. The following measurement was performed with the same scan range and without any correction of the lateral position [Fig. 11(b)]. The left two rows of cd pits visible in the original image [Fig. 11(a)] are again visible in the image shown in Fig. 11(b) after having removed and reinserted the sample. The slight lateral shift between the two images ($\Delta x=510$ nm, $\Delta y=140$ nm) is clarified in image Fig. 11(b) by an oval and the displacement vector Δs. A reproducibility of 1 μm is typical. Using the xy motor or an offset voltage applied to the scan piezo, the scanning area is easily readjusted to the original position.[75]

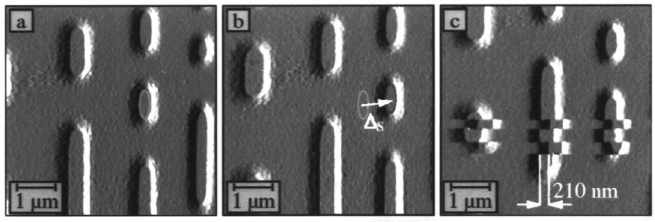

FIG. 11. Test of the sample mount and the xy motor. (a) Reference image, (b) image after removing and reinserting the sample, (c) test of xy motor.

In a second experiment we tested the operation of the xy motor. The measurement shown in Fig. 11(c) was scanned from left to right and from the bottom to the top of the image. At scan-line number 74 we have used the xy motor to make two steps into the negative x direction. This means that the SFM tip made two quantized movements to the left in addition to the homogeneous scanning motion of the sample. Clearly the imaged area has moved to the right side by about 210 nm. 15 scan lines later, two equally large steps into the positive x direction have moved the sample back to the original position. The procedure has been repeated at scan–line numbers 104 (again two steps into negative x direction) and 117 (again two steps into positive x direction). Note that the steps shown in Fig. 11(c) are the largest possible steps, one of them corresponding to a x movement of about 100 nm. The smallest step size may slightly depend on the condition of the instrument (vacuum or ambient, low temperature or ambient) but is smaller than 30 nm.

B. Test of dynamic and static measurement modes

First noncontact magnetic force microscopy experiments were performed on magneto-optically written bits in a 20 $\times$(5 Å $Co_{50}Ni_{50}$/5 Å Pt) multilayer (CAMST reference sample).[76] Due to the low squareness of the hysteresis loop, this material splits up into small domains which are still visible outside the bits. The bits were written with laser pulses of 0.24 μs duration and powers of 2.5, 5, 7.5, and 10 mW. Note that the bits are not fully saturated due to the low field applied during writing. We have used a Si_3N_4 cantilever with a force constant, $c_l=0.03$ N/m, and a resonance frequency, $f_0=12.5$ kHz. To obtain a tip with a well defined micromagnetic structure we have grown an electron beam

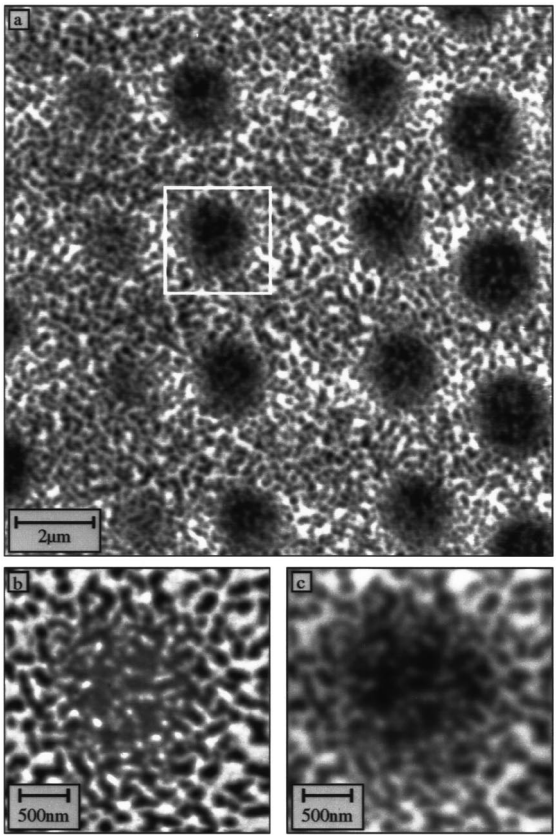

FIG. 12. Magnetic force microscopy images acquired on CAMST reference sample at room temperature. (a) Overview image acquired in air using a static SFM operation mode (variable deflection). (b) Dynamic mode (variable frequency) image acquired in vacuum. The white square in figure (a) indicates the location of image (b). (c) Simulation of a static mode image calculated from the MFM data (b).

induced deposition tip (EBID tip) onto the pyramid tip of the cantilever.[77,78] The EBID tip was coated with a 20-nm-thick layer of Co.

In Fig. 12(a) we present data acquired under ambient conditions using the variable deflection mode. The data was acquired in 34 min. To control the tip-to-sample distance we have applied an oscillating electric field with a frequency of 4 kHz between the tip and the sample.[79] Then, the 4 kHz component of the deflection of the cantilever was measured with a lock-in amplifier and kept constant by a feedback system adjusting the tip-to-sample distance. The image size is $14\,\mu\text{m}\times 14\,\mu\text{m}$ whereas the total force variation is 40 pN. Note that the signal-to-noise ratio is better than ten indicating that the minimal measurable force variation is below 4 pN which is comparable to values reached with our earlier instrumentation.[12]

Further data has been acquired with the same cantilever in vacuum on the same sample using a dynamic operation mode. We have used an analogue FM detector similar to Albrecht *et al.*[37] to measure the frequency variation (variable frequency mode). The tip-to-sample distance was kept constant as described above. Figure 12(b) shows a sized area within the original image, indicated by the white frame in Fig. 12(a). The total frequency variation is about 90 Hz. Using

$$\frac{\delta f}{f_0}=\frac{1}{2c_l}\cdot\frac{\partial F_z}{\partial z}, \tag{3}$$

where $c_l=0.03$ N/m is the force constant of the cantilever and $f_0=12.5$ kHz is the resonance frequency of the free cantilever, we calculate that a frequency variation of 90 Hz corresponds to a variation of the z derivative of the force of 4×10^{-4} N/m. Using a method described in Ref. 78 one can transform the dynamically measured data [Fig. 12(b)] into data [Fig. 12(c)] which would be acquired if the static cantilever deflection was measured at the same location and tip-to-sample distance. As described in more detail in Ref. 78, the small structures (high frequency components) are enhanced in the dynamic image [Fig. 12(b)] whereas the large structures (low frequency components) dominate in the static image [Fig. 12(c)]. Note that all structures visible in the *calculated data* [Fig. 12(c)] originating from data measured in the dynamic mode [Fig. 12(b)] can be found at the corresponding positions and with the correct force amplitude in the *measured data* acquired in the static operation mode [Fig. 12(a)].

C. Piezo calibration at variable temperatures

One of the difficulties in scanning probe microscopy originates from the rather complicated relation between the mechanical deformation of the piezo material used for scanning and the applied voltage. For one, this relation is not completely linear.[80,81] Furthermore, hysteretic behavior arising from piezo creep[82] considereably influences the scanning process.[83–85] Finally all these properties are strongly temperature dependent.[86,87]

Three different approaches have been discussed to overcome the above difficulties.

(1) Tamer and Dahleh[85] have measured the actual displacement of the piezo actuator *in situ* and corrected the nonlinear displacement via a feedback. Similar techniques are used today in commercially available scanning probe microscopes (SPMs).[88] Nevertheless this correction scheme is not used in our instrumentation, since the position measurement device has its own temperature dependence, needs additional space, and the electrical wiring of the device further complicates the construction of the microscope.
(2) A postmeasurement correction of the acquired data has been decribed in Refs. 89 and 90. In contrast to the first method such a postmeasurement correction of piezo nonlinearities does not require any position sensor within the instrument. However, the density of measurement points per unit sample area as well as the speed of the tip motion vary.
(3) Another approach for real-time correction is based on detailed, but not necessarily fundamental knowledge of the most important features of the dependence of piezo motion on the applied voltages. Once the response of the piezo upon the application of a linear voltage ramp is known, a feed forward correction of the ramp is used.

As indicated in Ref. 84, the amount of the lateral piezo motion, $d(U_{\max})$, upon ramping the voltage from a negative

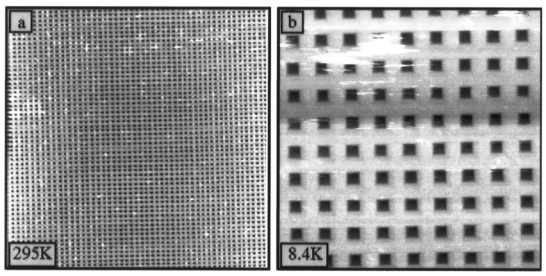

FIG. 13. Images of our calibration standard (Ref. 95) aquired in the variable deflection mode with the tip in contact with the sample. The paramaters for figure (a) are: $T=295$ K, $U_{max}=\pm 100$ V, $t_{scan}=0.2$ s, $d_{fast}=9.89$ μm, $d_{slow}=11.49$ μm, $\gamma_{fast}=0.88$, $\gamma_{slow}=0.84$. The paramaters for figure (b) are: $T=8.4$ K, $U_{max}=\pm 100$ V, $t_{scan}=0.2$ s, $d_{fast}=1.81$ μm, $d_{slow}=1.88$ μm, $\gamma_{fast}=0.99$, $\gamma_{slow}=0.98$.

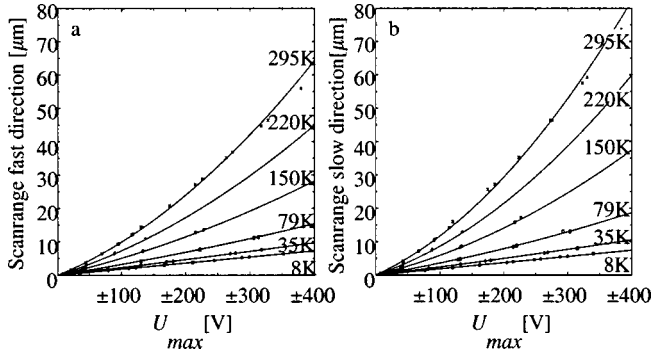

FIG. 14. Scan range, $d[\mu m]$, as a function of the maximum applied voltage, $U_{max}[V]$, and as a function of temperature, $T[K]$. (a) shows data and fit parabola for the fast scan direction whereas (b) shows the corresponding data and fits for the slow scan direction.

maximal value, $-U_{max}$ to a positive value $+U_{max}$ is best represented by a parabolic function[91] (A possible explanation for this behavior is described in Ref. 80):

$$d(U_{max},t_{scan},T)=\alpha(t_{scan},T)\cdot U_{max}+\beta(t_{scan},T)\cdot U_{max}^2. \quad (4)$$

The parameters α and β depend on the time per scanline, t_{scan},[92] and the temperature, T. As Eq. (4) indicates, a linear motion of the piezo with time requires a ''sublinear'' voltage ramp. In our experiments we find that

$$U(t,d,t_{scan},T)=U_{max}\cdot\left(\frac{t}{t_{scan}}\right)^{\gamma(d,t_{scan},T)} \quad (5)$$

is a suitable correction for a given temperature, T, maximum voltage, U_{max}, and scan time, t_{scan}. Note that the amount of nonlinearity is controlled by the paramter $\gamma(d,t_{scan},T)$ and that the voltage ramp becomes linear for $\gamma=1$. Solving Eq. (4) for U_{max} and replacing U_{max} in Eq. (5) leads to

$$U(t,d,t_{scan},T)=\frac{\alpha+\sqrt{\alpha^2+4\beta d}}{2\beta}\cdot\left(\frac{t}{t_{scan}}\right)^{\gamma}. \quad (6)$$

With a few limitations to be discussed below, the voltage ramp given in Eq. (6) leads to an almost distortion free image (see, e.g., Fig. 13) for an arbitrary scan range, d, and a given temperature, T. The functions $\alpha(t_{scan},T)$, $\beta(t_{scan},T)$ and $\gamma(t_{scan},T,U_{max})$ were determined experimentally.

Note, that the voltage ramp defined by Eq. (6) is the same for all scan lines. It is commonly known that the scan motion of the piezo strongly changes when the scanning motion is not in a stationary state, i.e., in the beginning of an image when the scanning motion has just been started, if the scan range has been changed considerably or if an offset voltage has been applied. Since Eq. (6) does not correct for these problems, we use the following techniques in addition: Before we start the aqcuisition of new data or after having changed the scan range, we leave the piezo scanning for at least a quarter of the time required to complete a full frame. Additionally, we avoid the use of a large offset voltage by positioning the center of the scanned area using the xy motor of our LTSFM.

The remaining problem is the determination of the functions $\alpha(t_{scan},T)$, $\beta(t_{scan},T)$, and $\gamma(t_{scan},T,U_{max})$ for our piezo scanner.[93] We performed the following set of measurements on a silicon calibration standard[94] at six temperatures, $T_i=8$, 35, 79, 150, 220, and 295 K. At each temperature we imaged the calibration standard with $U_{max,i}=\pm 100$, ± 200, ± 300, ± 400 V,[95] always adjusting the nonlinearity factor γ such that image distortion is minimal. This gives $\gamma(t_{scan,i},T_i,U_{max,i})$ (i running for all discrete temperatures and voltages). We then used the acquired images and Eq. (4) to determine $\alpha(t_{scan,i},T_i)$ and $\beta(t_{scan,i},T_i)$. Finally we found appropriate continuous functions, $\alpha(t_{scan},T)$, $\beta(t_{scan},T)$ and $\gamma(t_{scan},T,U_{max})$, to describe the descrete set of functions, $\alpha(t_{scan,i},T_i)$ and $\beta(t_{scan,i},T_i)$ and $\gamma(t_{scan,i},T_i,U_{max,i})$ for all temperatures, T, scan voltages, U_{max}, and scan times, t_{scan}.

Figure 13(a) shows an image of our calibration sample measured at room temperature. The applied maximum voltage, U_{max}, is ± 100 V, for both scan directions, the time per scanline is $t_{scan}=0.2$ s, the values for the nonlinearity correction are $\gamma_{fast}=0.88$ in the fast scan direction (from left to right), and $\gamma_{slow}=0.84$ in the slow scan direction (from bottom to top). Note that the image appears to be completely distortion free (i.e., the relative distances between two neighboring squares are constant for both scan directions throughout the whole image). However the scan range, d, is not the same for both scan directions ($d_{fast}=9.89$ μm, $d_{slow}=11.49$ μm). Since the scanning velocity of the piezo in the slow scan direction is a factor of 512 lower than in the fast scan direction, the strongly time dependent piezo creep leads to a larger motion of the piezo tube in the slow scan direction. The small rotation of the calibration pattern with respect to the scanning directions ($\approx 2°$) which can be seen more easy in Fig. 13(b) is due to a slight misalignment of the sample and the fact that no software scan rotation was used for the calibration measurements discussed.

Figure 13(b) shows an undistorted image of our calibration sample measured at 8.4 K but otherwise the same parameters as in Fig. 13(a). Comparing Figs. 13(a) and 13(b) one observes a reduction of the piezo sensitivity by a factor of about $5.5-6$[$d_{fast}(8.4\,K)=1.81$ μm, $d_{slow}(8.4\,K)=1.88$ μm), a reduction of piezo creep by 10% (the relative difference between d_{fast} and d_{slow} has reduced to about 4%), and a considerable reduction of nonlinearity (γ_{fast} is now 0.99 (RT value is 0.88) and γ_{slow} is now 0.98 (RT value is 0.84)].

Figure 14(a) shows the scan range, $d[\mu]$m, of our piezo scanner for the fast scan direction (scan time, $t_{scan}=0.2\,s$) as

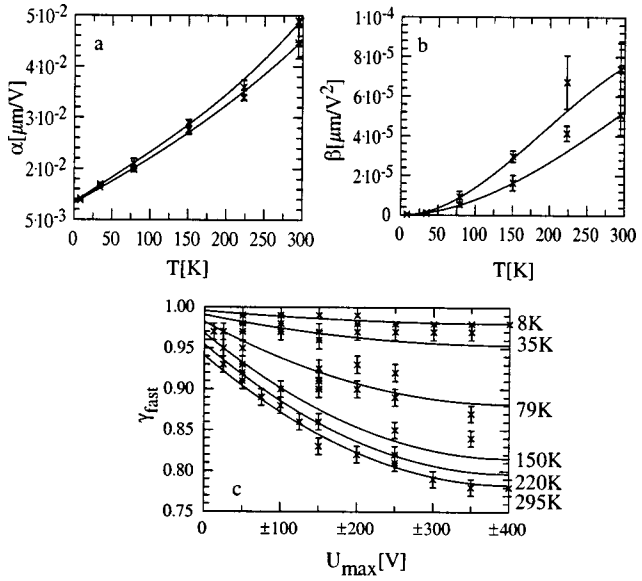

FIG. 15. Dependence of α, β, and γ from temperature, scan direction, and $U_{\max}$. (a) shows α as a function of temperature for the fast (lower curve) and the slow (upper curve) scan direction. (b) shows β as a function of temperature for the fast (lower curve) and the slow (upper curve) scan direction. (c) shows γ as a function of the applied maximum voltage, $U_{\max}$, and the temperature. The uppermost curve represents the behavior for the lowest temperature (8.4 K) indicating the lowest nonlinearity whereas the lowermost curve represents the behavior for the highest temperature (295 K) indicating maximum nonlinearity at RT.

a function of the applied voltage, $U_{\max}[V]$, for the discrete temperature values, T_i, mentioned above. The solid lines show the fit results with a quadratic polynom as given in Eq. (4). For all temperatures between these discrete temperatures, the functions $\alpha(t_{\text{scan}},T)$, and $\beta(t_{\text{scan}},T)$ provide the correct $d(U_{\max},T)$ dependence [Figs. 15(a) and 15(b)]. Figure 14(b) shows the corresponding data and fits for the slow scan direction. Note that the scan range of the slow scan direction is larger than the one of the fast direction for all scan voltages, temperatures, and scan speeds.[96] At room temperature and for the maximum scan voltage of $\pm 400\,V$ we find 64.2 μm for the fast and 82.1 μm for the slow scan direction. At 8 K this difference almost vanishes and we measure 7.2 and 7.4 μm, respectively. Furthermore, the averaged sensitivity of the piezo grows from 44.5 nm/V for a small scan voltage to 116 nm/V for the maximum scan voltage at room temperature for the fast scan direction. At 8 K the scan range versus maximum voltage function becomes more linear: We observe 8.97 and 9.12 nm/V, respectively.

The dependence of $\alpha[\mu\text{m/V}]$ and $\beta[\mu\text{m/V}^2]$ as a function of temperature, T[K], for our scanner is given in Figs. 15(a) and 15(b). In both cases, the lower curve represents the behavior in the fast scan direction whereas the upper curve gives the dependence for the slow scan direction, again indicating a higher piezo sensitivity in the slow scan direction. The dependence of γ_{fast} with respect to the applied maximum voltage, $U_{\max}$[V], and the temperature, T[K], are shown in Fig. 15(c). Here the uppermost curve (close to $\gamma=1$) is the low temperature curve ($T=8.4\,\text{K}$) whereas the lowermost curve represents room temperature data, indicating again the increasing nonlinearity of the piezo material with increasing temperature and increasing $U_{\max}$. Note that the strength of this procedure is that one does not need much theoretical knowledge about piezo behavior or information about specific piezo-ceramic constants to have a linearized scanner motion over a broad temperature range.

D. Test of the low temperature noise limit

The thermally activated noise density, $w_{th}(\omega)$, of a damped harmonic oscillator, e.g., a cantilever, is given in Ref. 97 as

$$w_{th}^2(\omega)=\frac{2\omega_0^3 k_B T Q}{c_l Q^2(\omega_0^2-\omega^2)^2+c_l\omega_0^2\omega^2},\quad [w_{th}]=\frac{\text{m}^2}{\text{Hz}}, \tag{7}$$

where ω_0 is 2π times the resonance frequency, f_0, Q is the quality factor, c_l the cantilever spring constant, k_B the Boltzmann constant, and T is the temperature. At resonance frequency ($\omega\approx\omega_0$), Eq. (7) simplifies to

$$w_{th}^2(\omega)\approx\frac{2k_B T Q}{c_l\omega_0},\quad [w_{th}]=\frac{\text{m}^2}{\text{Hz}}. \tag{8}$$

Note that the square of the noise density at the resonance frequency depends linearly on Q, whereas the width of the resonance peak is inversely proportional to Q. The thermally activated noise amplitude, $\langle x_{th}^2\rangle^{1/2}$, which is found by integration of $w_{th}^2(\omega)$ over the width of the resonance peak, is therefore independent of Q.

$$\langle x_{th}^2\rangle^{1/2}=\sqrt{\frac{2k_B T}{c_l}},\quad [\langle x_{th}^2\rangle^{1/2}]=\text{m}. \tag{9}$$

One finds (see Ref. 98) that the minimal measurable force derivative is

$$\frac{\partial}{\partial z}F_z\big|_{\min}=\frac{1}{A}\cdot\sqrt{\frac{4k_B T c_L B}{Q\omega_0}}, \tag{10}$$

where A is the oscillation amplitude of the cantilever and B is the measurement bandwidth.

Both, the increased instrumental stability allowing longer measurement times using smaller bandwidths, B, and the reduced thermal noise [Eq. (9)] result in an extremely small minimally measurable force derivative [Eq. (10)]. In Table I we summarize some values calculated for presently available cantilevers. Furthermore, it should be noted that even lower force derivatives or forces can be measured using specially fabricated supersoft cantilevers with high Q values.[99]

So far, only one group[100–103] has demonstrated reaching the thermodynamical limit. All others have either neglected this important test,[16] found no advantage to measurements performed at room temperature,[14] or have even failed to come within the correct order of magnitude.[104] While in the first two cases external noise may conspire to the thermally driven excitation of the cantilever, the strong heating of the piezo-resisitive cantilever may be the reason in the latter case. A careful description of the cantilever heating in the case of a piezo-resistive deflection sensor is found in Ref. 31.

As a first test, we have measured the frequency noise of a standard microfabricated monolithic Si cantilever from

TABLE I. $(\partial/\partial z)F_z|_{min}$ and δf_{min} as a function of the cantilever resonance frequency, f_0, the cantilever force constant, c_l, temperature, T. The calculations have been made for a cantilever quality factor, $Q=50\,000$, an oscillation amplitude, $A=1$ nm, and a measurement bandwidth, $B=1000$ Hz. If the oscillation amplitude, A, is increased by a factor of 10 (100), $\partial/\partial F_z|_{min}$ and δf_{min} decrease by a factor of 10 (100). If the measurement bandwidth, B, is decreased by a factor of 10 (100), $\partial/\zeta F_z|_{min}$ and δf_{min} are decreased by a factor of $\sqrt{10}$ (10).

f_0[kHz]	c_l[N/m]	T[K]	$\frac{\partial}{\partial z}F_z\Big\vert_{min}$ [N/m]	δf_{min}[Hz]
15	0.2	6	3.8×10^{-6}	0.14
15	0.2	295	2.6×10^{-5}	0.98
75	2	6	5.3×10^{-6}	0.10
75	2	295	3.7×10^{-5}	0.69
190	50	6	1.7×10^{-5}	0.03
190	50	295	1.2×10^{-4}	0.23
1000	50	6	7.2×10^{-6}	0.07
1000	50	295	5.1×10^{-5}	0.51

Nanosensors.[105] The front part of the backside of this cantilever was coated by a 40-nm-thick aluminum layer to increase its optical reflectivity. The front side was coated by a 10-nm-thick layer of iron to make the cantilever sensitive to magnetic stray fields. We have measured the resonance frequency of the free cantilever, $f_0=12\,016$ Hz. Using[106,107]

$$c_l = 15.96\left[\frac{\mathrm{Ns}^3}{\mathrm{m}^5}\right]\cdot b\cdot l^3\cdot f_0^3, \tag{11}$$

where b and l are the width and the length of the cantilever ($b=59\,\mu$m, $l=447\,\mu$m for the lever used here), we determine its spring constant to be 0.15 N/m. We have further measured the Q value, $Q\approx3600$ at a temperature $T=7.6$ K. Using Eq. (10), we determine the minimally measurable force derivative to be 1.23×10^{-6} N/m with a measurement bandwidth of 167 Hz.

For the lever described above, we measured a frequency noise of $\delta f=0.06$ Hz, using the analogue FM-detection system described in Sec. III. Using Eq. (3), we conclude that the measured noise of the force derivative is approximately 1.5×10^{-6} N/m, which matches the theoretical value of 1.23×10^{-6} N/m. Below we demonstrate that such a value is also reached during SFM measurements.

E. Low temperature measurements

As suggested before, both lateral resolution and sensitivity of the instrument has to be tested. An experiment aimed at atomic resolution (see Fig. 16) proves that a lateral resolution around an Angstroem is reached. However, atomic resolution images are inadequate to determine the force or force gradient sensitivity, because the forces in this type of experiment are in the nN range and force derivatives are in the high N/m range (see Refs. 108–114). In contrast, the typical interaction forces in magnetic force microscopy experiments are in the low pN range and the force derivatives are usually below 10^{-4} N/m (see Refs. 27,115,116,80).

Figure 17(a) shows raw data acquired at 7.6 K in noncontact variable force gradient mode on the CAMST reference sample.[76] The scan range is $6.9\,\mu\mathrm{m}\times6.9\,\mu$m, which is

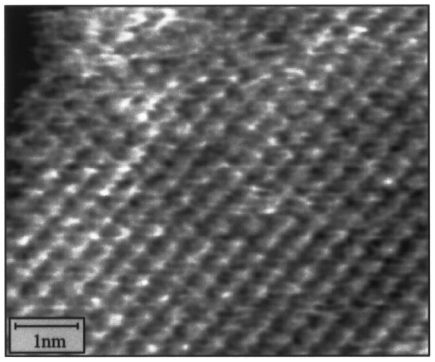

FIG. 16. Atomically resolved NaCl, measured at 7.6 K in variable deflection contact mode.

the maximum scan range at this temperature. The four bits visible, represent the bit-rows written with a laser power of 7.5 and 10 mW [see the two rows at the right side of Fig. 12(a)]. Panels (b) and (c) of Fig. 17 show raw data which were acquired at the locations marked by the white frames in panel (a). Note, that all details of Figs. 17(b) and 17(c) can be found identically and absolutely distortion free in the overview image, Fig. 17(a). This is due to the excellent stability and almost linearity of the scanning motion at low temperatures and to our precisely calibrated instrumentation. The cross-section in Fig. 17(d) shows that the total frequency variation is approximately 6 Hz, and that the signal-to-noise ratio (SNR) is around 100. This confirms the 0.06 Hz noise limit, which we have found above. Using Eq. (3), we can

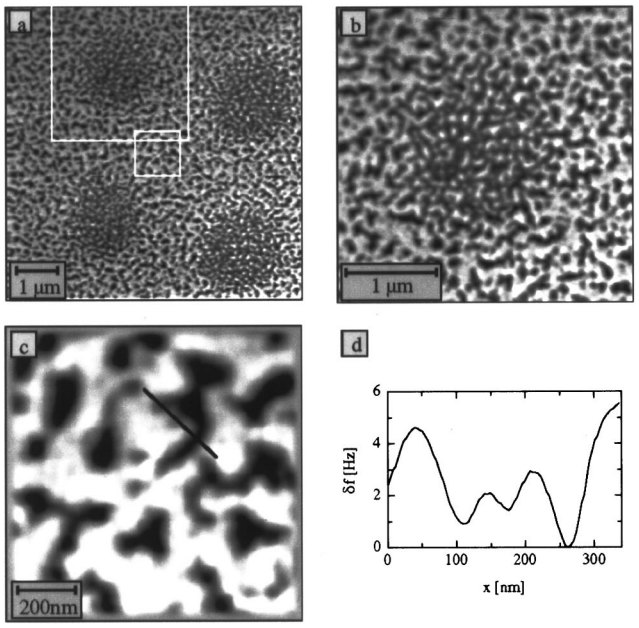

FIG. 17. Low temperature MFM data acquired on CAMST reference sample in dynamic noncontact variable gradient mode at $T=7.6$ K with a time per scanline (Ref. 117) of 4 s [(a) and (c) or 3.6 s (b)] and a pixel resolution of 512×512. (a) shows raw data with a scan range of 6.9 μm by 6.9 μm. One can see four magneto-optically written bits. (b) shows further raw data with a smaller scan range of 3.2 μm by 3.2 μm. This data was aquired within the area of the data shown in (a) as indicated by the big white square. (c) shows raw data with a scan range of 1 μm by 1 μm. Again this data was measured within the area of image (a) as indicated by the small white square. (d) shows a line section of the data shown in (c) along the direction indicated by the black line in (c).

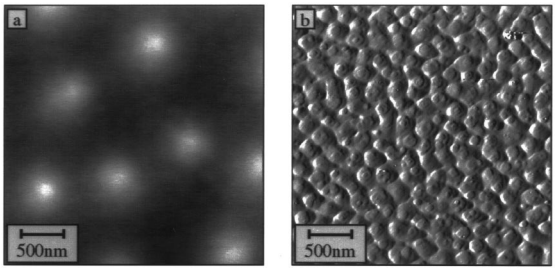

FIG. 18. Panel (a) shows the arrangement of eight vortices, generated while the $YBa_2Cu_3O_{7-x}$ thin film sample was field cooled in an external field of 2 mT. The total frequency shift within this data is 0.65 Hz. The signal to noise is about 10:1. The data was acquired in noncontact variable force gradient mode with a scan range of 3 μm by 3 μm and a time per scanline of 3 s. With the same tip we have measured the data shown in panel (b), acquired at the same sample location in noncontact constant force gradient mode. The original data was differentiated along the x direction. One can see the columnar structure typical for this material. One can also recognize single steps on top of these columns with a height of the unit cell of $YBa_2Cu_3O_{7-x}$.

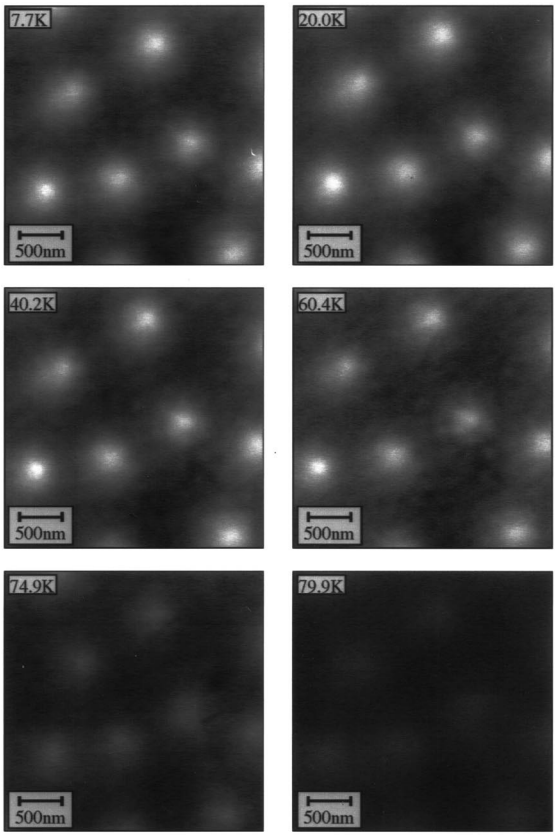

FIG. 19. All images are presented with the same greyscale which corresponds to a total frequency shift of 0.6 Hz. The small lateral drift (<1 μm) allows to image the same sample area for temperatures ranging from 7.7 to 79.9 K.

calculate that the total variation of the force derivative is equal to 1.9×10^{-4} N/m, while the smallest measureable force derivative is 1.9×10^{-6} N/m (for $f_0=13\,616$ Hz and $c_l=0.21$ N/m).

One of the most challenging applications for magnetic force microscopy is the direct imaging of vortices in the mixed state of a superconductor. So far only few data have been presented (see Refs. 28,27,31,32,35,117,118).

In Fig. 18(a) we present a 3 μm$\times$3 μm sized LTMFM image of vortices in a laser ablated YBCO thin film.[119] The number of vortices (≈8) corresponds well with the one expected in the imaged area for the field of 2 mT in which the sample was cooled (8.7). The MFM data was acquired at 7.6 K using the variable frequency operation mode. The total frequency variation is only 0.65 Hz corresponding to a z derivative of 2.1×10^{-5} N/m. Figure 18(a) shows raw data consisting of 512×512 measurement points acquired at a rate of 4s per line or 34 min per image. The SNR is approximately ten. This indicates that the minimal measurable force derivative is 2×10^{-6} N/m which is a similar value than the one reached in the measurement presented in Sec. III D. It is noteworthy that Volodin *et al.*[31,35] have reached a sensitivity which is high enough to image vortices by using higher flexure modes of their piezo-resistive cantilever. Although the SNR is approximately one, vortices in $NbSe_2$ single crystals are clearly imaged. In contrast, the LTSFM described in Ref. 32 achieves a force derivative resolution of 5×10^{-4} N/m. This is more than an order of magnitude larger than the critical limit for vortex imaging (2×10^{-5} N/m) and almost two orders of magnitude larger than the thermodynamical limit [For the used cantilever $f_0=60$ kHz, $c_l=2.5$ N/m, $T=6$ K, and $Q=3000$ one calculates 8×10^{-6} N/m].

In addition to the magnetic stray field we have measured the topography of the sample [Fig. 18(b)] at the same location. This is achieved by the following procedure: First the tip-to-sample distance is lowered until the frequency has shifted about 100 Hz. Then we activate a feedback system, which controls the tip-to-sample distance to keep the frequency shift constant during the following scan. Note, that this operation mode is commonly used in true atomic resolution experiments.[108–114] In our case we image a YBCO thin film, which was produced *ex situ* by laser ablation[119–122] with a tip coated by a ferromagnetic thin film to be sensitive for magnetic stray fields. Atomic resolution can therefore not be expected. However, unit cell steps of 1.2 nm are clearly visible and the growth island structure of these films is observed. This allows to correlate the position of the vortices with features of the topography. We will discuss further details in forthcoming publications.

Figure 19 shows an example for the variable temperature capabilities of the instrument. All images have a same scan range of 3 μm$\times$3 μm a number of pixels of 512×512, a scan speed of 3s per line and are presented with the frequency range of 0.6 Hz. All measurement temperatures were reached from below with a maximal overshoot of 0.1 K and kept constant during the measurement. Note, that we have observed only a small lateral drift (<1 μm) upon changing the temperature from 7.6 to 79.9 K. The vertical drift is probably due to the temperature sensitivity of the coated cantilever.[50–52] To avoid a tip crash during temperature changes, we have retracted the tip a few steps (some μm) before changing the temperature. We have used our methods presented above Sec. III C to realize the same scan range and distortion free images at all temperatures. Clearly, all images of Fig. 19 show the same arrangement of vortices. The contrast is reduced as the temperature is raised, as is expected from the divergence of the magnetic penetration depth, when

the critical temperature T_c is approached. Further details will be discussed in forthcoming publications.

ACKNOWLEDGMENTS

We would like to acknowledge the important contributions of Dr. A. Stephenson, presently at the Engineering Department, Cambridge University and Dr. J. Stroscio, National Institute of Standards and Technology to the development of the heatable sample holders. The authors also acknowledge Dr. B. Dam and Dr. A. Erb for providing the YBCO thin films and single crystals respectively. The CAMST reference sample has been kindly provided by the MESA Research Institute, University of Twente. A part of the work has been supported by the Swiss Priority Program NFP36.

[1] We give only a few citations as overview: See Refs. 121, 122.
[2] Citations are given in the successive text.
[3] The LTSFM system described here will be commercially available. It will be produced by Omicron Vakuumphysik GmbH, Idsteiner Str. 78, D-65232 Taunusstein.
[4] Mini CryoSTM, exchange gas cooled for temperatures between 1.5 and 300 K, produced by Oxford Instruments, Old Station Way, Eynsham, Witney Oxon, OX8 1TL.
[5] UHV Variable Temperture STM, for temperatures between 50 and 1000 K, produced by Oxford Instruments, Old Station Way, Eynsham, Witney Oxon, OX8 1TL.
[6] Low Temperature UHV STM, for temperatures around 5 K, produced by Omicron Vakuumphysik GmbH, Idsteiner Strasse 78, D-65232 Taunusstein, Germany.
[7] UHV Variable Temperture STM, for temperatures between 25 and 1500 K, produced by Omicron Vakuumphysik GmbH, Idsteiner Strasse 78, D-65232 Taunusstein, Germany.
[8] Usually the backside of the cantilever is coated by a thin metallic film to increase the optical reflectivity. Another example is the ferromagnetic coating needed to perform magnetic force microscopy experiments.
[9] F. Gießibl, C. Gerber, and G. Binnig, J. Vac. Sci. Technol. **9**, 984 (1991).
[10] A. Volodin and M. Marchevsky, Ultramicroscopy **42**, 757 (1992).
[11] T. Albrecht, P. Grütter, D. Rugar, and D. Smith, Ultramicroscopy **42–44**, 1638 (1992).
[12] H. Hug *et al.*, Rev. Sci. Instrum. **64**, 2920 (1993).
[13] K. Moloni, B. Moskowitz, and E. Dahlberg, Geophys. Res. Lett. **23**, 2851 (1996).
[14] R. Euler, U. Memmert, and U. Hartmann, Rev. Sci. Instrum. **68**, 1776 (1997).
[15] D. Pelekhov, J. B. Becker, and G. N. Nunes, Jr., Appl. Phys. Lett. **72**, 993 (1998).
[16] W. Allers, A. Schwarz, U. Schwarz, and R. Wiesendanger, Rev. Sci. Instrum. **69**, 221 (1997).
[17] C. Yuan *et al.*, Appl. Phys. Lett. **10**, 1308 (1994).
[18] Q. Dai *et al.*, Rev. Sci. Instrum. **66**, 5266 (1995).
[19] F. Gießibl and G. Binnig, Ultramicroscopy **42–44**, 281 (1992).
[20] H. Hug, T. Jung, and H.-J. Güntherodt, Rev. Sci. Instrum. **63**, 3900 (1992).
[21] D. Rugar *et al.*, Rev. Sci. Instrum. **59**, 2337 (1988).
[22] D. Rugar, H. Mamin, and P. Guethner, Appl. Phys. Lett. **55**, 2588 (1989).
[23] It should be noted that Rugar *et al.* still use a similar LTSFM for their extremely successful work on electron and nuclear spin resonance detection by magnetic force microscopy.
[24] A. Moser *et al.*, Meas. Sci. Technol. **4**, 769 (1993).
[25] H. Hug *et al.*, Physica B **194–196**, 377 (1994).
[26] A. Moser *et al.*, J. Vac. Sci. Technol. B **12**, 1586 (1994).
[27] A. Moser *et al.*, Phys. Rev. Lett. **74**, 1847 (1995).
[28] H. Hug *et al.*, Physica C **235–240**, 2695 (1994).
[29] H. Hug *et al.*, in *Forces in Scanning Probe Methods*, edited by H.-J. Güntherodt, D. Anselmetti, and E. Meyer, NATO ASI Series E: Applied Sciences (Kluwer, Dordrecht, 1995), Vol. 286.
[30] Private communication, D. P. E. Smith, NATO ASI on Scanning Force Microscopy, Schluchsee, Germany, 1994.
[31] A. Volodin and C. van Haesendonck, Appl. Phys. Lett. **73**, 1134 (1998).
[32] C. Yuan *et al.*, J. Vac. Sci. Technol. B **14**, 1210 (1996).
[33] Q. Lu, C.-C. Chen, and A. Lozanne, Science **276**, 2006 (1997).
[34] Based on our results published in Ref. 27 and methods presented in Ref. 80 we calculate the sensitivity necessary for vortex imaging to be about 5×10^{-6} N/m. Concluding from Ref. 17 the sensitivity of their instrument (5×10^{-4} N/m) might be too small to detect the stray field of single vortices. Furthermore, none of the tests proposed in Ref. 119 have been presented.
[35] A. Volodin, K. Temst, C. van Haesendonck, and Y. Bruynserasede, Appl. Phys. A: Solids Surf. (submitted).
[36] C. Prater *et al.*, J. Vac. Sci. Technol. B **9**, 989 (1991).
[37] T. Albrecht, P. Grütter, D. Horne, and D. Rugar, J. Appl. Phys. **69**, 668 (1991).
[38] This is necessary if the microscope has to be operated in fields up to 7 T.
[39] So far only one other LTSFM exists which is operated in the center of a superconducting magnet and has a xy-positioning device for the relative position of the cantilever with respect to the sample.
[40] H. Hug *et al.*, Omicron Newsletter **2**, Scientific Article (1998).
[41] http://www.omicron.de/products/cryo_sfm/, 1998.
[42] http://physics.nist.gov/Divisions/Div841/Gp3/epg_files/stm_lt_uhv.html, 1998.
[43] http://www.pc.chemie.uni-siegen.de/lieb/instrument.html.en, 1998.
[44] J. A. Heimberg *et al.*, Phys.-Techn. Bundesanstalt **PTB-F-30**, 25 (1997).
[45] Mechanical Hand (MH Series) from Vacuum Generators (VG), MEILI-Kryotech, Conradin-Zschokke Strasse 10, CH-5312 Döttingen, Switzerland, 1997.
[46] The cantilever runs from the $-Y$ to the $+Y$-direction.
[47] The wall also supports the electrical connectors of the instrument.
[48] Micro Slide Control Unit, Omicron Vakuumphysik GmbH, Idsteiner Strasse 78, D-65232 Taunusstein, Germany, 1998.
[49] S. Jarvis, A. Oral, T. Weihs, and J. Pethica, Rev. Sci. Instrum. **64**, 3515 (1993).
[50] J. Gimzewski, C. Gerber, E. Meyer, and R. Schlittler, Chem. Phys. Lett. **217**, 589 (1994).
[51] E. Meyer, J. K. Gimzewski, Ch. Gerber, and R. R. Schlittler, *Micromechanical Calorimeter with Picojoule Sensitivity*, edited by M. E. Welland and J. K. Gimzewski (Kluwer, Dordrecht, 1995), p. 89.
[52] R. Berger *et al.*, Appl. Phys. Lett. **69**, 40 (1996).
[53] HPT Translator from Vacuum Generators (VG), MEILI–Kryotech, Conradin-Zschokke Strasse 10, CH-5312 Döttingen, Switzerland, 1997.
[54] ISE 10 Sputter Cleaning Ion Source, Omicron Vakuumphysik GmbH, Idsteiner Strasse 78, D-65232 Taunusstein, Germany, 1997.
[55] Triple EFM, 3-cell UHV Evaporator, Omicron Vakuumphysik GmbH, Idsteiner Strasse 78, D-65232 Taunusstein, Germany, 1997.
[56] This keeps the length of all wires and the optical fiber constant during the vertical translation of the SFM.
[57] These clamps are also needed to remove the load from the spring suspension of the SFM when the system is baked.
[58] L. Salerno, P. Kittel, and A. Spivak, AIAA J. **22**, 1810 (1984).
[59] K.-H. Yoo and A. Anderson, Cryogenics **23**, 531 (1983).
[60] We normally use a separate laboratory turbomolecular pumping system for this purpose.
[61] KF means Klammerflansch according to the product catalogue of Balzers.
[62] Oxygen free high conductivity copper.
[63] Cryostat, custom-made for Dr. H. J. Hug by Oxford Instruments, Old Station Way, Eynsham, Witney Oxon, OX8 1TL, 1993.
[64] The definition of OFHC is oxygen free high conductivity copper.
[65] Note that the bottom part of the UHV tube cannot be made solely from an electrically well conducting material since an accidental quench of the superconducting magnet would then induce high Eddy currents which may crush the SFM section.
[66] This temperature is measured with the temperature sensor described in Sec. II A 3.
[67] Note that the relatively high viscosity of the LN_2 makes it difficult to pump enough LN_2 through the needle valve to achieve sufficient cooling. Furthermore, the needle valve shows a strong tendency to freeze when LN_2 is used as a coolant.
[68] In the future we plan to reach an even lower base temperature by modifying the baffles of the cryostat insert to lower the heat load onto the cones.
[69] K. Jülich Ferienkurs, *Magnetisimus von Festkörpern und Grenzflächen* (Springer, New York, 1993).
[70] MagLab-CMP, a cantilever magnetometer system, produced by Oxford Instruments, Old Station Way, Eynsham, Witney Oxon, OX8 1TL.

[71] H. J. Hug *et al.*, Rev. Sci. Instrum. **64**, 2920 (1993).
[72] H. Hug *et al.*, Physica B **12**, 1591 (1994).
[73] Note that this is rather trivial for contact measurements since they usually rely on the strong repulsive force between tip and sample. However in noncontact measurements, the z derivative, may change sign. When the sign of the z derivative of the interaction force changes, the feedback system tries to correct an error by changing the tip-to-sample distance into the wrong direction.
[74] C. Loppacher *et al.*, Appl. Phys. A: Solids Surf. **66**, 215 (1998).
[75] Note that the precision of the exchange mechanism is of crucial importance for the cantilever. The cantilever is adjusted on its holder *ex situ* by means of a dummy stage. Afterwards the cantilever holder is mounted into the SFM without further coarse adjustments.
[76] *CAMST Topical Meeting on Magnetic Force Microscopy* (MESA Research Institute, The Netherlands, 1995).
[77] M. Rührig *et al.*, J. Appl. Phys. **79**, 2913 (1996).
[78] H. J. Hug *et al.*, J. Appl. Phys. **83**, 5609 (1998).
[79] The frequency was chosen to be high enough not to disturb the static measurement of the cantilever deflection which was acquired in the 0–500 Hz frequency band.
[80] J. Akia and S. Wadhwa, Rev. Sci. Instrum. **66**, 2517 (1995).
[81] R. Emch, P. Descouts, and P. Niedermann, J. Microsc. **152**, 85 (1988).
[82] T. Jung, Ph.D. thesis, Universität Basel, 1992.
[83] T. Yokohata, S. Hara, R. Kaneko, and K. Kato, Jpn. J. Appl. Phys., Part 1, **33**, 1209 (1994).
[84] E. Riis *et al.*, Appl. Phys. Lett. **54**, 2530 (1989).
[85] N. Tamer and M. Dahleh, Proceedings of the 33rd Conference on Decision and Control **2**, 1826 (1994).
[86] K. Vandervoort, R. Zasadzinski, G. Galicia, and G. Crabtree, Rev. Sci. Instrum. **64**, 896 (1993).
[87] M. Locatelli and G. Lamboley, Rev. Sci. Instrum. **59**, 661 (1988).
[88] True Metrix, real-time closed loop correction for piezo scanner nonlinearities, Trademark of TopoMetrix Corporation, 5403 Betsy Ross Drive, Santa Clara, CA 95054-1162.
[89] L. Hadjiiski, S. Münster, E. Oesterschulze, and R. Kassing, J. Vac. Sci. Technol. B **14**, 1563 (1996).
[90] C. Cai, X. Chen, Q. Shu, and X. Zheng, Rev. Sci. Instrum. **63**, 5649 (1992).
[91] Where d means the scan range of the piezo tube in μm, and $U_{\max}$ is the corresponding Voltage applied to the scanner.
[92] t_{scan} is here defined as the time for one scan direction within a single scan line (forward or backward). If an equal scanning speed for both scan directions is chosen, the total time per scan line is therefore $2 \cdot t_{\text{scan}}$.
[93] We use an EBL2 scanner with an outer diameter of 12.7 mm and a length of 38.1 mm.
[94] The calibration standard is an etched silicon wafer, which has quadratic etch pits arranged in a quadratic lattice. The pits have a sidelength of 100 nm, a spacing of 200 nm, and a depth of 70 nm.
[95] For instance ± 100 V means that bipolar voltages are applied to opposite segments of the piezo scanner, resulting in a total voltage difference of 200 V.
[96] This is also the case if one interchanges the fast and the slow scan directions. In fact we found no assymetry between the x- and y-piezo electrodes.
[97] C. Heer, *Statistical Mechanics, Kinetic Theory, and Stochastic Processes* (Academic, New York, 1992).
[98] T. Albrecht, P. Grütter, D. Horne, and D. Rugar, J. Appl. Phys. **69**, 668 (1991).
[99] T. Stowe *et al.*, Appl. Phys. Lett. **71**, 288 (1997).
[100] D. Rugar, C. Yannoni, and J. Sidles, Nature (London) **360**, 563 (1992).
[101] J. Sidles and D. Rugar, Phys. Rev. Lett. **70**, 3506 (1993).
[102] O. Züger and D. Rugar, Appl. Phys. Lett. **63**, 2496 (1993).
[103] K. Wago *et al.*, J. Vac. Sci. Technol. B **14**, 1197 (1996).
[104] In Ref. 17 the minimally measured force derivative is 5×10^{-4} N/m while one calculates a value of 8×10^{-6} N/m for the used cantilever ($f_0 = 60$ kHz, $c_l = 2.5$ N/m, $T = 6$ K and $Q = 3000$).
[105] Nanosensors, Dr. Olaf Wolter GmbH, IMO–Building, Im Amtmann 6, D-35578 Wetzlar-Blankenfeld, Germany.
[106] M. Bammerlin, Master's thesis, Universität Basel, 1995.
[107] M. Nonnemacher, Ph.D. thesis, Universität Sindelfingen, 1990.
[108] F. Gießibl, Science **267**, 68 (1995).
[109] P. Güthner, J. Vac. Sci. Technol. B **14**, 2428 (1995).
[110] S. Kitamura and M. Iwatsuki, Jpn. J. Appl. Phys., Part 1, **34**, 145 (1995).
[111] H. Ueyama, M. Ohta, Y. Sugawara, and S. Morita, Jpn. J. Appl. Phys., Part 1, **34**, 1086 (1995).
[112] R. Luethi *et al.*, Z. Phys. B **100**, 165 (1996).
[113] S. Kitamura and M. Iwatsuki, Jpn. J. Appl. Phys., Part 1, **35**, 668 (1996).
[114] L. Olsson, R. Wigren, and R. Erlandson, Rev. Sci. Instrum. **67**, 8309 (1996).
[115] G. Bochi *et al.*, Phys. Rev. Lett. **75**, 1839 (1995).
[116] H. Hug *et al.*, J. Appl. Phys. **79**, 5609 (1996).
[117] The total time per scanline, i.e., for forward plus backward movement.
[118] A. Moser, H. Hug, B. Stiefel, and H.-J. Güntherodt, J. Magn. Magn. Mater. **190–192**, 114 (1998).
[119] B. Dam *et al.*, Physica C **261**, 1 (1996).
[120] D. Eigler and E. Schweizer, Nature (London) **344**, 524 (1990).
[121] H. Hess *et al.*, J. Vac. Sci. Technol. A **8**, 450 (1990).
[122] G. Meyer, Rev. Sci. Instrum. **67**, 2960 (1996).